fibers

MDPI

Article

Solution Blow Spinning to Prepare Preferred Oriented Poly(ethylene oxide) Submicrometric Fibers

Javier González-Benito [1,2,*], Miguel A. Lorente [1], Dania Olmos [1,2] and Ana Kramar [1,2]

[1] Department of Materials Science and Engineering and Chemical Engineering, University Carlos III of Madrid, 28911 Leganés, Spain
[2] Institute of Chemisty and Materials Technology, IQMAAB, Universidad Carlos III de Madrid, 28911 Leganés, Spain
* Correspondence: javid@ing.uc3m.es

Abstract: In this work, materials with potential biomedical applications constituted by fibrous poly(ethylene oxide), PEO, are prepared by solution blow spinning (SBS). The SBS setup has a cylindrical collector for which the rotational speed and size are varied to study its effect on the final morphology of the materials. The morphology is inspected using field emission scanning electron microscopy and studied using image analysis. As a result, many doubts were generated because of the use of different methods of image analysis, therefore a simpler and more conventional method using Image J open-source software was used to ensure the accuracy of the final interpretation. It is shown that fiber size and orientation depend on the linear speed associated with the surface of the collector more than on its rotational speed; therefore, it can be said that the morphology of materials prepared by SBS will depend on the size, shape, and rotational speed of the collector. When the linear speed of the cylindrical collector increases, fibers get thinner, less entangled, and more oriented. It is clear, therefore, that the linear speed of material collection by solution blow spinning is a very important parameter of processing to control the final morphology of materials manufactured by that method. Since morphology can affect the final properties of the materials the simple variation of the linear speed might have important implications on their final performance for different biomedical applications.

Keywords: solution blow spinning; poly(ethylene oxide); PEO; morphology; nanofibers

Citation: González-Benito, J.; Lorente, M.A.; Olmos, D.; Kramar, A. Solution Blow Spinning to Prepare Preferred Oriented Poly(ethylene oxide) Submicrometric Fibers. *Fibers* **2023**, *11*, 79. https://doi.org/10.3390/fib11090079

Academic Editor: Shingo Yokota

Received: 7 August 2023
Revised: 7 September 2023
Accepted: 20 September 2023
Published: 21 September 2023

1. Introduction

The morphology and topography of materials can highly influence their final properties. Among others, mechanical properties [1], wettability [2,3], adhesion, and differentiation of cells can be affected. A particular case is constituted by fibrous materials since fibers present a high aspect ratio which leads to a higher impact of the preferential orientation on the final morphology and even topography [4].

Nowadays there exists a great interest in finding materials that are easy to prepare and, if possible, are able to be dispensed on particular sites or in situ (for instance on the skin), to improve tissue regeneration in the case of wound dressings, or tissue engineering in the case of scaffolds. From a clinical point of view, among other characteristics these materials should have: (a) good coupling or direct contact with the surface of the tissue in general or the wound in particular; (b) ease for transporting nutrients; (c) ability of absorption and even extraction of the exudate; (d) biocompatibility and biodegradability and (e) easy to promote correct adhesion of cells, if necessary, differentiation and subsequent tissues development.

To date, there are many techniques for the preparation of supports for tissue growth (scaffolds). Those processing techniques should allow for well-controlled architectures, morphologies, or microstructures to be obtained, so that they can even mimic the structures of the living tissues themselves [5]. Among the most commonly used processing methods

are those that involve a selective solution of heterogeneous polymer-based materials, for instance, when water-soluble salts are used to fill polymers [6–10], they can be highlighted. Other kinds of methods involve the preparation of materials constituted by very thin fibers that can mimic the geometry of the extranuclear matrix found in certain tissues, thus they are able to stimulate cell adhesion and growth which are essential to enhance tissue regeneration [11,12]. Among those methods, electrospinning (ES) and solution blow spinning (SBS) are receiving special attention. ES is a technique from which materials are constituted mainly by submicrometric fibers are usually obtained. In this technique, a polymer solution is injected in a capillary by the action of a pump while the capillary is connected to a ground which will act as a collector of the material produced. Once a voltage difference between the capillary and the collector is applied, a high electric field is generated that will interact with the polymer solution coming out from the capillary to stretch it and generate fibers if the proper conditions are chosen. In solution blow spinning, a polymer solution is injected with the aid of a pump and a syringe and then stretched and projected on a collector by the action of a pressurized gas. This process is similar to electrospinning although in this case, however the driving force for stretching the solution is an intense electric field instead of a pressurized gas which makes it less versatile for the preparation of materials. Recently [13–16], our research group has provided the adaptation of an SBS device initially proposed by Medeiros et al. [17,18]. The main difference introduced is that our device is completely automatized through the use of an Arduino microchip controlled by an Android device and that the nozzle can move from left to right parallel to the long axis of the cylindrical collector to ensure homogeneity of the materials prepared in terms of their thickness.

Although ES and SBS can produce fibers of very small diameters, when compared to each other, both have their advantages and disadvantages. The main advantage of ES is that the fibers generated have greater homogeneity in terms of morphology and size. However, ES seems to present some disadvantages that must be considered for certain applications. ES devices have a very low ability for their adaptation when in situ deposition of materials is required, for example on wounds. In addition, in ES it is usually necessary to apply large electric fields between the material dispenser and the collector along with the need for the solvents and materials used to possess special properties that allow them to properly interact with the electric field. Finally, for proper nanofibrillar material manufacturing, ES requires very low polymer solution feeding rates with the consequence of having low production rates. All these difficulties might be solved with the use of SBS; perhaps with the only difficulty of finding the adequate process conditions to obtain the required fibrillar morphology.

Apart from fibrillar microstructures, there is also a lot of interest in supports with oriented morphology. In particular, it is known that the regeneration of highly ordered structures such as those associated with tendons and ligaments can only be carried out effectively in supports ("scaffolds") that can provide a topographic guide for cells [19]. In fact, since extracellular matrices are formed by organized collagen fibers, many studies have been carried out on the effect of fiber alignment which were obtained using electrospinning on several types of cells [20,21]. It is evident that the existence of an intense electric field in ES is a factor favoring the preferential orientation; however, as mentioned above the sole feeding rate of the solution might be a disadvantage for scaling up the process. Due to this, other methods such as using SBS to produce fibers, should be investigated for the same purpose. During the last five years, research on materials constituted by submicrometric fibers prepared using solution blow spinning has increased considerably [22,23]. Although, in general, organic polymer-based materials are prepared by SBS, such as neat polymers [24,25] and composites [26,27], inorganic materials can be also obtained, as recent articles show, for instance, carbon nanofibers from poly acrylonitrile, PAN, and lignin [28], and more recently Nb_2O_5 sub-micrometric fibers from metal oxide precursor nanoparticles [29]. However, a few works have been focused on the use of SBS [30] and ES [31,32] to obtain fibrous materials where their constituted fibers show preferential orientations. How-

ever, the distributions of the reported preferred orientations of fibers might be confusing since the analysis is usually based on very complicated methods of image analysis [31,32] in which the results depend on previous preparation of the image and the parameters chosen to carry out the analysis. For this reason, apart from proposing new methods of preparing materials constituted by fibers with tailored orientations, it is necessary to show clear and comprehensive methods of image analysis to yield quantitative and semiquantitative information from parameters that are easy to understand in terms of the particular morphological characteristics of the material.

Among the materials that gather most of the characteristics required for its implementation in biomedical applications, poly(ethylene oxide), PEO, is one of the most known and used. Apart from its biocompatibility, its solubility in water makes it biodegradable and therefore very useful for the controlled release of drugs [33,34]. The PEO can be easily synthesized with different molar masses, allowing in that way to have a wide range of properties. Thanks to its hydrophilicity, it is soluble in water although with different behaviors depending on its molecular weight and crystallinity degree. Besides, it is neither toxic nor sensitive to pH and physiological fluids. On the other hand, PEO presents the ability to be processed using SBS to obtain non-woven mats constituted by submicrometric fibers as it is reflected in other works [1,35,36].

In this study, the method of fabricating poly(ethylene oxide)-based materials via solution blow spinning are described. In order to modify the fibrillar morphology of the materials, the size (smaller and larger collector denoted as S and L, respectively) and rotation speed (ranging from 200 RPM to 1000 RPM) of the cylindrical collector used in the solution blow spinning were varied. To thoroughly investigate the effects of these factors on the morphology of the collected material, a careful analysis of microscopic images was undertaken. This analysis culminated in the derivation of parameters that facilitate the straightforward interpretation of quantitative morphological details. Consequently, these parameters contribute significantly to a deeper comprehension of the material's microstructural attributes and overall characteristics, which advances the understanding of its potentiality for many properties and applications.

2. Materials and Methods

2.1. Materials

The materials are prepared from poly(ethylene oxide) (PEO) (powder, Mv = 100,000, CAS: 25322-68, density = 1.13 g/mL). Polymeric solutions required for solution blow spinning were prepared by dissolving the PEO in a solvent mixture of acetone, Ac (CAS: 67-64-1, Mw = 58.08 g/mol, bp = 56 °C, density = 0.791 g/mL) and chloroform, Chf (CAS: 67-66-3, Mw = 119.38 g/mol, bp = 61 °C, density = 1.48 g/mL) in a 1:1 volume ratio.

2.2. Samples Preparation

Most of the processing conditions, among others, the solvent system, the concentration of the solution, the dimensions of the nozzle, and the air pressure were chosen based on previous results which demonstrated the feasibility of obtaining PEO fibers by SBS [1]. Polymer solutions were blow spun with a homemade device [1,37]. In this particular work, PEO solutions with a concentration of 10% by weight per unit of volume (w/v) were injected with a syringe at a feeding rate FR of 0.5 mL/min in a capillary (inner and outer diameters of the capillary 0.8 mm and 1.0 mm, respectively) which constitutes the inner channel of a concentric nozzle. Pressurized air at a pressure of 2 atm is simultaneously passed through the outer channel of the nozzle (diameter 2.0 mm). The liquid solution that comes out from the nozzle is stretched by the action of the pressurized air while simultaneously, the solvent evaporates while heading towards the collector, leading to fibers (if adequate SBS conditions are used) that travel a distance of 15 cm (working distance, WD) until they reach a rotating cylindrical collector with a particular rotational speed, RS. In the SBS set-up, the protrusion distance of the capillary with respect to the exit of the concentric nozzle was set at 5 mm, while the collector was a solid cylinder covered with aluminum foil where the material was

deposited. To ensure thickness and homogeneity of the mat collected, the collector rotates as the nozzle moves parallelly to the long axis of the cylindrical collector at a constant rate (200 or 1000 rpm). After dispensing at least 20 mL of PEO solution, nonwoven mats of PEO were carefully removed from the aluminum foil and cut to get square specimens to be inspected by microscopy. On the other hand, materials were prepared at room conditions of 20–25 °C, 1 atm of pressure, and a relative humidity of 35–45%. To confirm there was not any trace of solvents remaining in the materials attenuated total reflectance Fourier transformed infrared spectroscopy (ATR-FTIR) was used.

In order to change the preferential orientation of the microconstituents of the materials two variables were considered for the SBS processing conditions, the size of the collector (in terms of its diameter, Dc) and the rotational speed of the collector, RS. Two different collectors were considered, a large cylindrical collector, L, with a diameter of 6.5 cm, and a small cylindrical collector, S, with a diameter of 2.0 cm. On the other hand, two RS were considered: 200 rpm and 1000 rpm. Table 1 shows sample codes depending on the values of the variables considered, Dc and RS respectively. From the size of the cylindrical collector and the rotational speed in revolutions per minute (rpm), the linear speed in $m{\cdot}s^{-1}$, v, of the collector when rotating was calculated following Equation (1) and also gathered in Table 1.

$$v\left(m{\cdot}s^{-1}\right) = \omega\left(rad{\cdot}s^{-1}\right){\cdot}r(m) \quad (1)$$

where ω is the angular velocity in radians per second, r is the radius of the collector in meters and 1 rpm corresponds to $2\pi/60 = 0.1047$ ($rad{\cdot}s^{-1}$).

Table 1. Sample codes and SBS processing variables.

Sample Code	Collector Diameter, D_c (cm)	Rotational Speed, RS (rpm)	v ($m{\cdot}s^{-1}$)
S-200	2.0	200	0.21
L-200	6.5	200	0.68
S-1000	2.0	1000	1.05
L-1000	6.5	1000	3.40

2.3. Equipments

The morphology of the materials prepared was studied using field emission scanning electron microscopy via a TENEO field emission scanning electron microscope (FESEM-FEI) using an electron acceleration voltage of 5kV. Square specimens were mounted on aluminum stubs using a double adhesive carbon tape and then, to avoid electrostatic charge accumulation, the samples were carbon coated through an evaporation process using a Leica EM ACE200 low-vacuum coater. Digital images were obtained from the data generated by the signal arising from secondary electrons (SE) detected by an Everhart-Thornley (ETD) detector. Before assuming the morphology of the fibers along the thickness of the samples is the same, some experimental evidence should be given. One option can be to analyze cross-section images of the sample and the other one is to use different tilts to obtain the SEM images. In this second case, we can also reach other interesting information that would correspond to the consideration that there is not any optical artifact that might affect the dimensions of the fibers in the case that the images obtained at different tilts would be used to obtain stereoscopic images. Therefore, for a particular specimen, several images were taken at different tilt angles (−5°, 0°, 5° and 10°) to have more (almost 3D) information regarding the morphology.

For ATR-FTIR analysis a Nicolet iS5 (Thermo Scientific, Thermofisher, Waltham, MA, USA) spectrometer equipped with an ATR device with diamond window GladiATR (PIKE Technologies, Fitchburg, WI, USA) was used. The spectra were collected from the average of 32 scans in a wavenumber range from 400 cm^{-1} to 4000 cm^{-1} and a resolution of 4 cm^{-1}.

2.4. Digital Image Analysis

The free software ImageJ was used to carry out the image analysis. Digital images obtained by FESEM were imported by the ImageJ 1.53t (Wayne Rasband & contributors, National Institute of Health, Bethesda, MD, USA) and the morphology was analyzed by the tool "measure" and the plugin "Ridge detection" to obtain distributions of fibers diameters and orientations and fibers joins, respectively. In order to avoid any kind of confusion the fiber size, through their diameters, and orientations was manually measured and taken randomly in at least 80 locations for measurment. To ensure a random choice of sites for the measurements, a virtual grid (yellow dashed lines in Figure 1) was positioned over the image and the locations to make the measurements were chosen as the intersections between the virtual lines of the grid and the fibers. As an example, on the SEM image of Figure 1 magenta lines represent the corresponding measurements of diameters, and green lines the directions used to obtain angle orientations of the fibers. For the measurements of orientations, it is important to highlight those lines on the fibers must always be drawn following a particular criterium for instance from left to right. As an example, Figure 2 shows schematically two hypothetical measurements of fiber orientation in terms of angles at 45° and −45° respectively.

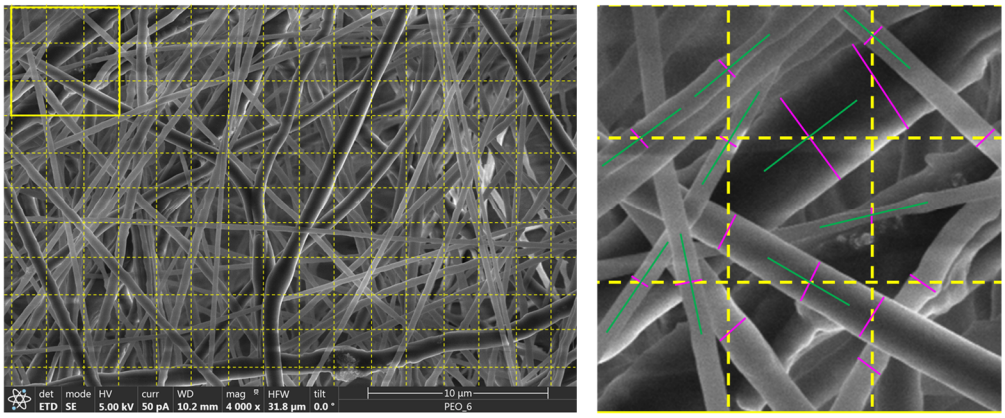

Figure 1. Example of SEM image analysis to measure diameters and orientation of fibers. The whole SEM image (**left**) and zoomed region are represented by the yellow square in the whole image with measurements (**right**). Yellow dashed lines represent the grid used to guide in the choice of fibers on which to perform measurements and green and magenta lines are examples of segments drawn to make measurements.

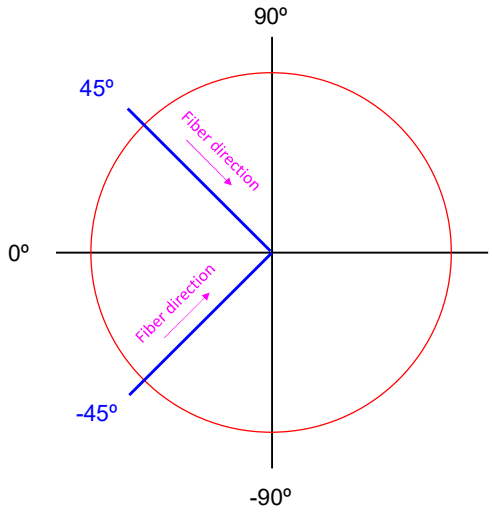

Figure 2. Schematical representation of two hypothetical measurements of fiber orientation in terms of angles at 45° and −45°.

Finally, all measurements were represented as a distribution using a bar diagram from which different parameters were obtained: the average of the distribution and the standard deviation. On the other hand, all distributions were fitted by multi-gaussian functions to extract other parameters such as the maxima of the distribution, mainly for comparison purposes.

Fiber joins are considered as the number of intercrossing points between fibers. This parameter was obtained using the plugin "Ridge detection" of the software ImageJ. Since this parameter depends on several initial conditions to make the calculation, certain care should be taken when interpreting results. The Ridge Detection plugin for the software Image J is a tool that allows detecting lines that in our case are associated with fibers, which is based on the algorithm described in reference [38]. When those lines intersect each other, the corresponding breakpoints are stored as joins. There are several parameters to choose in order to make the corresponding calculations and that is the reason why different results might be obtained. They can be divided into mandatory and optional parameters respectively. In the first case, the parameters are (a) Sigma: It depends on the line width and is used to control the scale at which ridges are detected in an image; (b) Lower Threshold: is the minimum intensity threshold for a pixel to be considered part of the line; (c) Upper Threshold: is the maximum intensity threshold for a pixel to be considered part of the line and (d) Darkline (yes/no), this parameter determines whether dark or bright lines are considered for the simulation. For more information, the reader can go to the website of the free software ImageJ 1.53t (https://imagej.net/, accessed on 7 September 2023). Considering the variety of parameters, it is expected to have different results depending on the values chosen. However, if the analysis for all the images were performed following the same path and criteria at least a qualitative interpretation of the results can be done.

3. Results

The morphology of the differently prepared materials was inspected by FESEM. Figure 3 shows the images at several magnifications corresponding to the different materials under study. It can be seen that the materials are very homogeneous with respect to their microstructure, being mainly constituted by fibers with diameters ranging from 50 nm to 1000 nm. Distributions of fiber's size in terms of their diameters are also shown in Figure 3. From the top to the bottom of the FESEM images of Figure 3, the images were put in order depending on their linear speeds (from lower to higher) used to collect the materials. Apart from the appearance of thinner fibers it can be seen that the higher the collection speed the narrower the size distributions are, pointing out that the diameter or size homogeneity increases as the collection speed increases. On the other hand, it can be clearly seen that the higher the linear velocity of the collector the less twisted or curved the fibers are.

The images were also quantitatively analyzed to obtain the size distribution of fibers in terms of their diameters (see Figure 3). Regarding the quantitative aspect of size distribution, (see Figure 3 on the right) it is important to highlight that this analysis was carried out for the images obtained using different tilt angles in the microscope, obtaining distributions in the form of histograms for each tilt from the measurement of at least 80 diameters per image. This was performed in order to involve as many fibers as possible in the measurement. Considering that the image analysis with ImageJ gives information in only two dimensions, when results arising from the analysis of images obtained are combined from different tilts, a better approximation to the reality is achieved since it is an indirect way of considering the third dimension of the materials i.e., in fact the nanofibrous mats prepared have certain thickness. In each case the average of the distribution was calculated, D_T, as well as the corresponding standard deviation, *std*, being gathered in Table 2 as $D_T \pm std$. As can be seen, regardless of the material, there is not any trend with the tilt angle; therefore, all diameters measured per material were incorporated into a unique distribution (distributions shown in Figure 3) from which a global average diameter was obtained, $<D>$, together with its corresponding standard deviation, σ (Table 2). In this

case, a general trend for those values can be seen whereby the average diameter slightly decreases and the width of the distribution (standard deviation) clearly decreases as the linear speed of the collector increases, indicating, as it was mentioned before, that fibers get thinner and more homogeneous the higher the velocity used to collect the material.

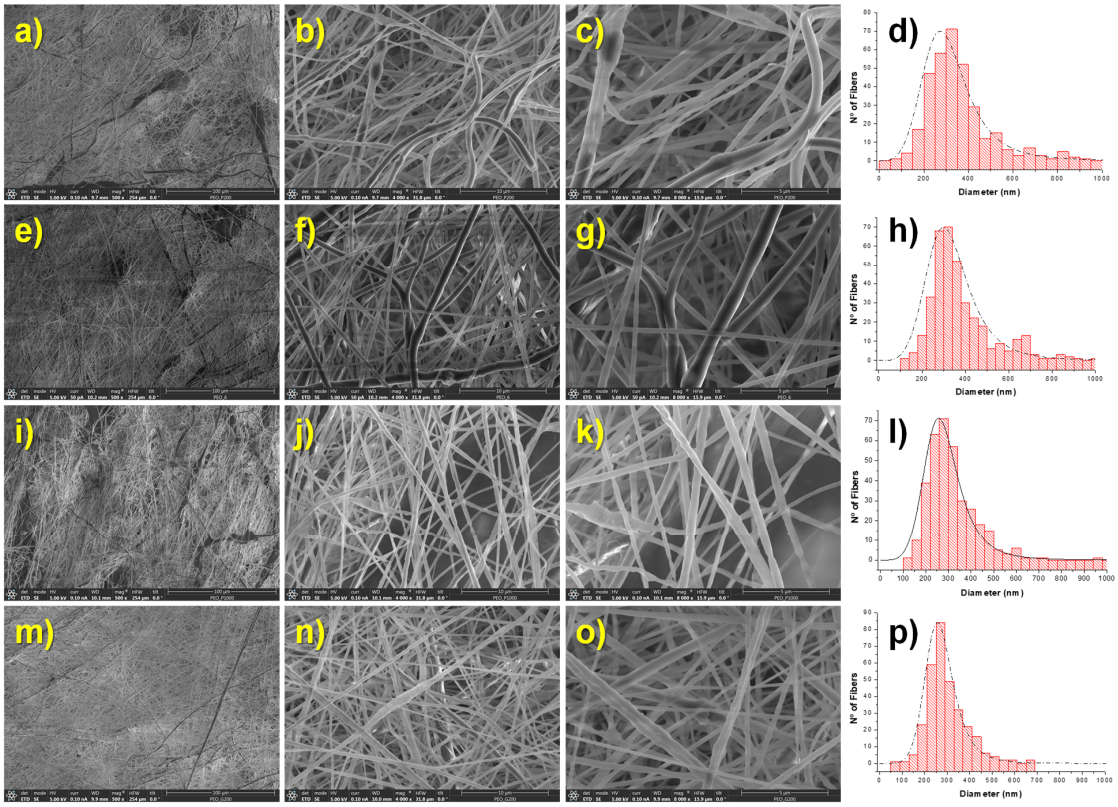

Figure 3. Diameter distributions and SEM images at different magnifications corresponding to the different materials prepared. (**a**–**d**) images and diameters distribution corresponding to the sample S-200; (**e**–**h**) images and diameters distribution corresponding to the sample L-200; (**i**–**l**) images and diameters distribution corresponding to the sample S-1000 and (**m**–**p**) images and diameters distribution corresponding to the sample L-1000.

Table 2. Values of parameters used to characterize fiber size and mat density for the different PEO-based samples.

Sample (Tilt)	v (m/s)	Tilt (°)	Joins	<Joins>	D_T (nm)	<D> (nm)	σ (nm)	D_{max} (nm)	$<D_{max}>$ (nm)
S-200 (−5)	0.21	−5	205	196 ± 41	394 ± 290	383	223	290	271
S-200 (0)		0	221		351 ± 163			253	
S-200 (5)		5	135		412 ± 279			280	
S-200 (10)		10	221		375 ± 161			289	
L-200 (−5)	0.68	−5	299	270 ± 38	390 ± 176	386	160	253	298
L-200 (0)		0	214		394 ± 166			271	
L-200 (5)		5	278		386 ± 139			307	
L-200 (10)		10	287		375 ± 162			289	
S-1000 (−5)	1.05	−5	209	206 ± 10	337 ± 110	316	105	268	256
S-1000 (0)		0	192		343 ± 118			273	
S-1000 (5)		5	211		314 ± 106			256	
S-1000 (10)		10	213		314 ± 114			246	
L-1000 (−5)	3.40	−5	67	91 ± 25	279 ± 75	297	83	239	253
L-1000 (0)		0	73		300 ± 100			230	
L-1000 (5)		5	106		295 ± 76			250	
L-1000 (10)		10	117		317 ± 97			264	

On the other hand, using the plugin "Ridge Detection" with the software ImageJ, the number of joins between fibers was estimated (Table 2). Although the use of this plugin highly depends on the image, as well as its quality and level of brightness and contrast, it can be considered a good method to have at least semiquantitative data of joins (interconnections between fibers). In Table 2 it can be seen there is a tendency for the number of joins to decrease as the linear speed to collect the materials increases. This result can give other interesting information about the porosity of the materials since, if there is simultaneously a decrease in the size of fibers and the number of joins, it could be concluded that the porosity must increase with fewer and larger pores.

Another important morphology feature that can highly influence the performance of these fibrous materials is the preferred orientation of the microconstituents, in this particular case, the fibers for the samples under study. In Figure 4, the distributions of fiber orientations for each material are represented in terms of the number of fibers (counts) with a certain orientation expressed in terms of angles between -90° to 90° and their corresponding cumulative plots. In general, a clear alignment of fibers was not observed but this result is simply due to some limitations that the solution blow spinning technique still presents, which is expected to be resolved in the near future with other device designs. With SBS the air can change the flow direction when it reaches the solid collector, which is the reason why some fibers may attach to the surface of the collector in a random manner without following the direction imposed by the rotation of the collector.

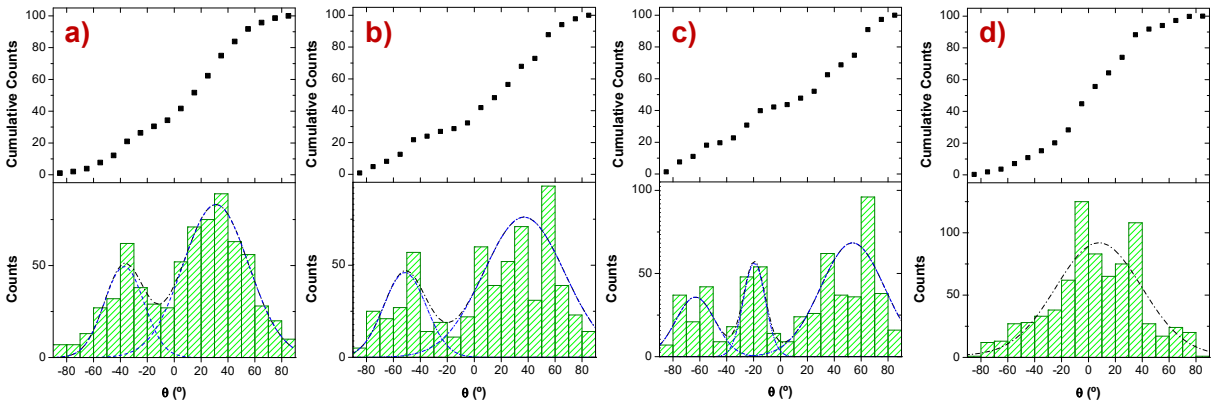

Figure 4. Distributions of fiber orientations for each material: (**a**) S-200; (**b**) L-200; (**c**) S-1000 and (**d**) L-1000.

However, as can be seen in Figure 4, using the three lowest rotation rates of the collector the fibers are deposited following multimodal distributions while, when the highest rotation rate is used (Material L-1000) fibers are deposited following a monomodal distribution, indicating, at least for this last material, a clearer preferential orientation of fibers.

In principle, a bimodal distribution might be expected considering the way the fibers are collected. In Figure 5, a scheme that explains how bimodal distributions for fiber orientations are obtained is shown. The nozzle moves parallel to the long axis of the cylindrical collector which rotates following a perpendicular direction. Therefore, when the nozzle moves to the right, one range of angles for the fiber deposition on the collector will be favorable while, when the nozzle moves to the left the other range of angles would be favorable.

As the rotation speed increases, less difference should be observed between the two preferential orientations until the rotational speed of the collector (drum) is so fast that it collects fibers with a preferential orientation conditioned exclusively by it. This reason would justify why the fiber's orientation distributions can be well fitted by two Gaussians (Figure 4) that apparently separate from each other (in fact, the distributions get closer to each other because of the periodical character of the representation) when the rotation

speed of the collector increases until in between them it is necessary to add a third Gaussian to fit the distribution. Finally, when the rotational speed of the collector is high enough only one Gaussian is the dominant, leading to a clear and unique preferential orientation of fibers.

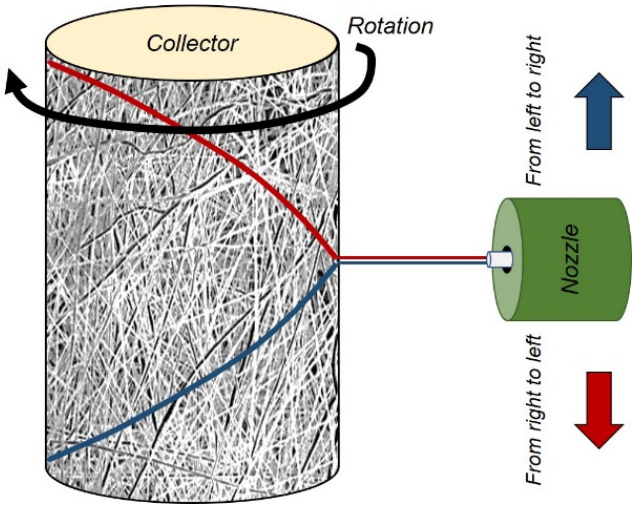

Figure 5. Representative scheme showing how bimodal distributions of fiber orientations are obtained from the solution blow spinning setup used in this work.

In order to better interpret these results, Table 3 gathers some parameters extracted from the distributions. For example, the average orientation angle per sample and tilt used to obtain the FESEM images, θ_T. As can be seen, regardless of the material, there is not any clear trend with the tilt angle; therefore, all angles measured per material were incorporated into a unique distribution (distributions shown in Figure 3) from which it was obtained a global average angle per sample (all tilts are included for the statistical calculation), <θ>, its corresponding standard deviation, σ_θ, and the maxima corresponding to the Gaussians, were used to deconvolute the orientation angles distributions, θ_{max}, together with their widths and areas in brackets.

Table 3. Values of the parameters used to describe the preferential orientation of fibers constituting the different PEO-based samples.

Sample (Tilt)	v (m/s)	Tilt (°)	θ_T (°)	<θ> (°)	σ_θ (°)	θ_{max} (Width, Area) (°)
S-200 (−5)	0.21	−5	82 ± 56	62	53	143 (29, 1823)
S-200 (0)		0	77 ± 55			31 (58, 5076)
S-200 (5)		5	67 ± 53			
S-200 (10)		10	67 ± 57			
L-200 (−5)	0.68	−5	75 ± 53	70	50	130 (37, 1526)
L-200 (0)		0	72 ± 51			37 (71, 4692)
L-200 (5)		5	68 ± 50			
L-200 (10)		10	67 ± 47			
S-1000 (−5)	1.05	−5	79 ± 63	88	49	117 (34, 1231)
S-1000 (0)		0	91 ± 63			161 (20, 1100)
S-1000 (5)		5	86 ± 67			54 (56, 3739)
S-1000 (10)		10	89 ± 71			
L-1000 (−5)	3.40	−5	95.9 ± 36	95	34	96 (76, 7577)
L-1000 (0)		0	95.5 ± 37			
L-1000 (5)		5	95.2 ± 33			
L-1000 (10)		10	94.3 ± 30			

As can be interpreted from Figure 4 and Table 3, as the velocity of collector rotation to collect the fibers increases, the distribution of fiber orientations broadens because the two preferential orientations become more distinguishable from each other. However,

considering the periodic character of the representations, what is occurring is just the opposite, this behavior would be easily observed if the distributions corresponding to each material (Figure 4) were represented showing periodicity in the same graph, for instance, repeating the distributions every 180°. In this way, to make the calculations and to obtain the corresponding quantitative parameters (Table 2) the range from 0° to 180° of the periodic representation was used instead of the range from −90° to +90°.

4. Conclusions

In this work, it was shown that the morphology and distribution of nanofibers produced using solution blow spinning are highly dependent on the linear speed of the collector used. It was proven that fiber size and orientation depend on the linear speed associated with the surface of the collector more than its rotational speed. When the linear speed of the cylindrical collector increases, fibers get thinner, less entangled and curly, and more oriented. It is clear therefore, that the linear speed of material collection by solution blow spinning is a very important parameter of processing to control the final morphology of materials and then their final properties and performance regarding their potential for biomedical applications. Moreover, it has been shown that in the case of a nozzle moving parallel to the long axis of the rotation of the collector, a bimodal distribution of fiber orientation is present. If the linear speed of the collector increases, the bimodal distribution of fiber orientations broaden i.e., the two preferential orientations become more distinguishable from each other, and finally, when the linear speed is much faster than the nozzle horizontal movement, the distinguishable bimodal distributions are fused into one broad, which means that preferential orientation is monomodal.

Regarding the way through which the fiber's size and orientation have been analyzed, it can be said that the method chosen is consistent and provides significant results from the analysis of just a single image of the fibrous material, thus reducing analysis time no matter what way the image is acquired.

Author Contributions: Conceptualization, J.G.-B.; methodology, J.G.-B.; software, M.A.L. and J.G.-B.; validation, J.G.-B.; formal analysis, M.A.L. and J.G.-B.; investigation, M.A.L. and J.G.-B.; resources, J.G.-B.; data curation, J.G.-B.; writing—original draft preparation, M.A.L. and J.G.-B.; writing—review and editing, M.A.L., D.O., A.K. and J.G.-B.; visualization, M.A.L. and J.G.-B.; supervision, J.G.-B.; project administration, J.G.-B.; funding acquisition, J.G.-B. All authors have read and agreed to the published version of the manuscript.

Funding: This research was funded by AEI (Ministerio de Ciencia e Innovación of Spain, PID2020-112713RB-C21 and -C22), the Universidad Carlos III de Madrid, Fondos de Investigación of Fco. Javier González Benito [2012/00130/004] and the strategic Action in Multifunctional Nanocomposite Materials [Code: 2011/00287/003].

Data Availability Statement: The data presented in this study are available on request from the corresponding author.

Acknowledgments: Participation of A.K. working under the CONEX-Plus program of Universidad Carlos III de Madrid (UC3M) and the European Commission through the Marie-Sklodowska Curie COFUND Action (Grant Agreement No 801538).

Conflicts of Interest: The authors declare no conflict of interest.

References

1. Lorente, M.Á.; González-Gaitano, G.; González-Benito, J. Preparation, Properties and Water Dissolution Behavior of Polyethylene Oxide Mats Prepared by Solution Blow Spinning. *Polymers* **2022**, *14*, 1299. [CrossRef] [PubMed]
2. Kasiri, A.; Domínguez, J.E.; González-Benito, J. Morphology optimization of solution blow spun polystyrene to obtain superhydrophobic materials with high ability of oil absorption. *Polym. Test.* **2020**, *91*, 106859. [CrossRef]
3. Domínguez, J.E.; Kasiri, A.; González-Benito, J. Wettability behavior of solution blow spun polysulfone by controlling morphology. *J. Appl. Polym. Sci.* **2021**, *138*, 50200. [CrossRef]
4. Fan, J.; Zhang, Y.; Liu, Y.; Wang, Y.; Cao, F.; Yang, Q.; Tian, F. Explanation of the cell orientation in a nanofiber membrane by the geometric potential theory. *Results Phys.* **2019**, *15*, 102537. [CrossRef]

5. Prasad, A.; Sankar, M.R.; Katiyar, V. State of Art on Solvent Casting Particulate Leaching Method for Orthopedic ScaffoldsFabrication. *Mater. Today Proc.* **2017**, *4*, 898. [CrossRef]
6. Guarino, V.; Causa, F.; Taddei, P.; di Foggia, M.; Ciapetti, G.; Martini, D.; Fagnano, C.; Baldini, N.; Ambrosio, L. Polylactic acid fibre-reinforced polycaprolactone scaffolds for bone tissue engineering. *Biomaterials* **2008**, *29*, 3662. [CrossRef]
7. Santana-Melo, G.F.; Rodrigues, B.V.M.; da Silva, E.; Ricci, R.; Marciano, F.R.; Webster, T.J.; Vasconcellos, L.M.R.; Lobo, A.O. Electrospun ultrathin PBAT/nHAp fibers influenced the in vitro and in vivo osteogenesis and improved the mechanical properties of neoformed bone. *Colloids Surf. B Biointerfaces* **2017**, *155*, 544. [CrossRef]
8. Rodrigues, B.V.M.; Razzino, C.A.; de Carvalho Oliveira, F.; Marciano, F.R.; Lobo, A.O. On the design and properties of scaffolds based on vertically aligned carbon nanotubes transferred onto electrospun poly (lactic acid) fibers. *Mater. Des.* **2017**, *127*, 183. [CrossRef]
9. Rodrigues, B.V.M.; Silva, A.S.; Melo, G.F.S.; Vasconscellos, L.M.R.; Marciano, F.R.; Lobo, A.O. Influence of low contents of superhydrophilic MWCNT on the properties and cell viability of electrospun poly(butylene adipate-co-terephthalate) fibers. *Mater. Sci. Eng. C* **2016**, *59*, 782. [CrossRef]
10. Roseti, L.; Parisi, V.; Petretta, M.; Cavallo, C.; Desando, G.; Bartolotti, I.; Grigolo, B. Scaffolds for bone tissue engineering: State of the art and new perspectives. *Mater. Sci. Eng. C* **2017**, *78*, 1246. [CrossRef]
11. Rim, N.G.; Shin, C.S.; Shin, H. Current approaches to electrospun nanofibers for tissue engineering. *Biomed. Mater.* **2013**, *8*, 014102. [CrossRef] [PubMed]
12. Chong, E.J.; Phan, T.T.; Lim, I.J.; Zhang, Y.Z.; Bay, B.H.; Ramakrishna, S.; Lim, C.T. Evaluation of electrospun PCL/gelatin nanofibrous scaffold for wound healing and layered dermal reconstitution. *Acta Biomater.* **2007**, *3*, 321. [CrossRef] [PubMed]
13. Iorio, M.; Teno, J.; Nicolás, M.; García-González, R.; Peláez, V.H.; González-Gaitano, G.; González-Benito, J. Interfacial Conformations and Molecular Structure of PMMA in PMMA/Silica Nanocomposites. Effect of High-Energy Ball Milling. *Colloid Polym. Sci.* **2018**, *296*, 461. [CrossRef]
14. Teno, J.; González-Gaitano, G.; González-Benito, J. Poly (ethylene-co-vinyl acetate) films prepared by solution blow spinning: Surface characterization and its relation with E. coli adhesión. *Polym. Test.* **2017**, *60*, 140. [CrossRef]
15. González-Benito, J.; Teno, J.; González-Gaitano, G.; Xu, S.; Chiang, M.Y. PVDF/TiO2 nanocomposites prepared by solution blow spinning: Surface properties and their relation with S. Mutans adhesión. *Polym. Test.* **2017**, *58*, 21. [CrossRef]
16. Teno, J.; González-Gaitano, G.; González-Benito, J.J. Nanofibrous polysulfone/TiO2 nanocomposites: Surface properties and their relation with E. coli adhesión. *Polym. Sci. Part B Polym. Phys.* **2017**, *55*, 1575. [CrossRef]
17. Medeiros, E.S.; Glenn, G.M.; Klamczynski, A.P.; Orts, W.J.; Mattoso, L.H.C. Solution blow spinning: A new method to produce micro- and nanofibers from polymer solutions. *J. Appl. Sci.* **2009**, *113*, 2322. [CrossRef]
18. Medeiros, E.S.; Glenn, G.M.; Klamczynski, A.P.; Orts, W.J.; Mattoso, L.H.C. Solution Blow Spinning. U.S. Patent 8,641,960 B1, 4 February 2014.
19. Shang, S.; Yang, F.; Cheng, X.; Frank Walboomers, X.; Jansen, J.A. The effect of electrospun fibre alignment on the behaviour of rat periodontal ligament cells. *Eur. Cells Mater.* **2010**, *19*, 180. [CrossRef]
20. Chew, S.Y.; Mi, R.; Hoke, A.; Leong, K.W. Aligned protein-polymer composite fibers enhance nerve regeneration: A potential tissue engineering platform. *Biomaterials* **2008**, *29*, 653. [CrossRef]
21. Huaqiong, L.; Feng, W.; Huizhi, C.; Mintu, P.; Yuekun, L.; Allan, Z.Z.; Lay, P.T. Micropatterning extracellular matrix proteins on electrospun fibrous substrate promote human mesenchymal stem cell differentiation toward neurogenic lineage. *ACS Appl. Mater. Interfaces* **2016**, *8*, 563.
22. Gao, Y.; Zhang, J.; Su, Y.; Wang, H.; Wang, X.; Huang, L.; Yu, M.; Ramakrishna, S.; Long, Y. Recent Progress and Challenges in Solution Blow Spinning. *Mater. Horiz.* **2021**, *8*, 426. [CrossRef] [PubMed]
23. Gomes de Castro Monsores, K.; Oliveira da Silva, A.; de Sant' Ana Oliveira, S.; Pondé Weber, R.; Lopes Dias, M.J. Production of nanofibers from solution blow spinning (SBS). *Mater. Res. Technol.* **2022**, *16*, 1824. [CrossRef]
24. Dong, W.; Liu, F.; Zhou, X.; Wang, L.; Zhao, Z.; Zhou, Y.; Li, H.; Liu, Q.; Deng, B.; Li, D. Superhydrophilic PVDF nanofibrous membranes with hierarchical structure based on solution blow spinning for oil-water separation. *Sep. Purif. Technol.* **2022**, *301*, 121903. [CrossRef]
25. Dadol, G.C.; Lim, K.J.A.; Cabatingan, L.K.; Tan, N.P.B. Solution blow spinning–polyacrylonitrile–assisted cellulose acetate nanofiber membrane. *Nanotechnology* **2020**, *31*, 345602. [CrossRef] [PubMed]
26. Popkov, A.V.; Kulbakin, D.E.; Popkov, D.A.; Gorbach, E.N.; Kononovich, N.A.; Danilenko, N.V.; Stankevich, K.S.; Choynzonov, E.L.; Zheravin, A.A.; Khlusov, I.A. Solution Blow Spinning of PLLA/Hydroxyapatite Composite Scaffolds for Bone Tissue Engineering. *Biomed. Mater.* **2021**, *16*, 055005. [CrossRef]
27. Ye, B.; Jia, C.; Li, Z.; Li, L.; Zhao, Q.; Wang, J.; Wu, H.J. Solution-blow spun PLA/SiO2 nanofiber membranes toward high efficiency oil/water separation. *App. Polym. Sci.* **2020**, *137*, 49103. [CrossRef]
28. Camargo de Gonzaga, L.A.; Martins, M.C.F.; Correa, A.C.; Facchinatto, W.M.; da Silva, C.M.P.; Colnago, L.A.; Mattoso, L.H.C. Production of carbon nanofibers from PAN and lignin by solution blow spinning. *J. Polym. Res.* **2021**, *28*, 237. [CrossRef]
29. Silva, V.D.; Medeiros, E.S.; Macedo, D.A.; Simões, T.A. Engineering of Nb2O5 sub-micrometric fibers from metal oxide precursor nanoparticles by Solution Blow Spinning. *Ceram. Int.* **2023**, *49*, 15649. [CrossRef]
30. Kobuszewska, A.; Kolodziejek, D.; Wojasinski, M.; Jastrzebska, E.; Ciach, T.; Brzozka, Z. Lab-on-a-chip system integrated with nanofiber mats used as a potential tool to study cardiovascular diseases (CVDs). *Sens. Actuators B Chem.* **2021**, *330*, 129291. [CrossRef]

31. He, H.; Wang, Y.; Farkas, B.; Nagy, Z.K.; Molnar, K. Analysis and prediction of the diameter and orientation of AC electrospun nanofibers by response surface methodology. *Mater. Des.* **2020**, *194*, 108902. [CrossRef]
32. Dorati, R.; Chiesa, E.; Pisani, S.; Genta, I.; Modena, T.; Bruni, G.; Brambilla, C.R.M.; Benazzo, M.; Conti, B.J. The effect of process parameters on alignment of tubular electrospun nanofibers for tissue regeneration purposes. *Drug Deliv. Sci. Technol.* **2020**, *58*, 101781. [CrossRef]
33. Knop, K.; Hoogenboom, R.; Fischer, D.; Schubert, U.S. Poly(ethylene glycol) in drug delivery: Pros and cons as well as potential alternatives. *Angew. Chem.* **2010**, *23*, 6288. [CrossRef] [PubMed]
34. Ma, L.; Deng, L.; Chen, J. Applications of poly(ethylene oxide) in controlled release tablet systems: A review. *Drug. Dev. Ind. Pharm.* **2014**, *40*, 845. [CrossRef] [PubMed]
35. Lorente, M.; González-Gaitano, G.; Valero, M.; González-Benito, J. Solution Blow Spun Poly(ethylene oxide)/Poly-ε-caprolactone System: Properties and Dissolution in Water. *ACS Appl. Polym. Mater.* **2023**, *5*, 6562. [CrossRef]
36. Oliveira, J.E.; Mattoso, L.H.C.; Orts, W.J.; Medeiros, E.S. Structural and morphological characterization of micro and nanofibers produced by electrospinning and solution blow spinning: A comparative study. *Adv. Mater. Sci. Eng.* **2013**, *2013*, 1. [CrossRef]
37. Domínguez, J.E.; Olivos, E.; Vázquez, C.; Rivera, J.M.; Hernández-Cortes, R.; González-Benito, J. Automated low-cost device to produce sub-micrometric polymer fibers based on blow spun method. *HardwareX* **2021**, *10*, e00218. [CrossRef]
38. Steger, C. An Unbiased Detector of Curvilinear Structures. *IEEE Trans. Pattern Anal. Mach. Intell.* **1998**, *20*, 113. [CrossRef]